

RESEARCH ARTICLE

10.1002/2014GC005344

Key Points:

- Most extensive hydrothermal plume survey anywhere on the mid-ocean ridge
- Hydrothermal frequency tracks magmatic budgets at regional and segment scales
- Plume clusters and MBA lows imply a melt lens beneath 14–33% of the ridge axis

Supporting Information:

- Readme
- Tables S1–S3

Correspondence to:

E. T. Baker,
edward.baker@noaa.gov

Citation:

Baker, E. T., C. Hémond, A. Briais, M. Maia, D. S. Scheirer, S. L. Walker, T. Wang, and Y. J. Chen (2014), Correlated patterns in hydrothermal plume distribution and apparent magmatic budget along 2500 km of the Southeast Indian Ridge, *Geochem. Geophys. Geosyst.*, 15, 3198–3211, doi:10.1002/2014GC005344.

Received 17 MAR 2014

Accepted 15 JUL 2014

Accepted article online 17 JUL 2014

Published online 19 AUG 2014

Correlated patterns in hydrothermal plume distribution and apparent magmatic budget along 2500 km of the Southeast Indian Ridge

Edward T. Baker^{1,2}, Christophe Hémond³, Anne Briais⁴, Marcia Maia³, Daniel S. Scheirer⁵, Sharon L. Walker¹, Tingting Wang^{6,7}, and Yongshun John Chen⁶

¹NOAA Pacific Marine Environmental Laboratory, Seattle, Washington, USA, ²Now at Joint Institute for the Study of the Atmosphere and Ocean—PMEL, University of Washington, Seattle, Washington, USA, ³Laboratoire Domaines Océaniques, Université de Brest, CNRS-UBO, Plouzane, France, ⁴CNRS, Geosciences and Environment Toulouse, University of Toulouse, Toulouse, France, ⁵US Geological Survey, Menlo Park, California, USA, ⁶School of Earth and Space Sciences, Peking University, Beijing, China, ⁷Now at School of Ocean and Earth Science, Tongji University, Shanghai, China

Abstract Multiple geological processes affect the distribution of hydrothermal venting along a mid-ocean ridge. Deciphering the role of a specific process is often frustrated by simultaneous changes in other influences. Here we take advantage of the almost constant spreading rate (65–71 mm/yr) along 2500 km of the Southeast Indian Ridge (SEIR) between 77°E and 99°E to examine the spatial density of hydrothermal venting relative to regional and segment-scale changes in the apparent magmatic budget. We use 227 vertical profiles of light backscatter and (on 41 profiles) oxidation-reduction potential along 27 first and second-order ridge segments on and adjacent to the Amsterdam-St. Paul (ASP) Plateau to map p_h , the fraction of casts detecting a plume. At the regional scale, venting on the five segments crossing the magma-thickened hot spot plateau is almost entirely suppressed ($p_h = 0.02$). Conversely, the combined p_h (0.34) from all other segments follows the global trend of p_h versus spreading rate. Off the ASP Plateau, multisegment trends in p_h track trends in the regional axial depth, high where regional depth increases and low where it decreases. At the individual segment scale, a robust correlation between p_h and cross-axis inflation for first-order segments shows that different magmatic budgets among first-order segments are expressed as different levels of hydrothermal spatial density. This correlation is absent among second-order segments. Eighty-five percent of the plumes occur in eight clusters totaling ~350 km. We hypothesize that these clusters are a minimum estimate of the length of axial melt lenses underlying this section of the SEIR.

1. Introduction

Submarine hydrothermal venting occurs where a heat source exists and permeability is sufficient to sustain fluid circulation in the crust. At the global scale, the spatial density of vent sites is strongly correlated with spreading rate, a proxy for the long-term magmatic budget [e.g., Baker and German, 2004]. At the segment scale, the existence of high-temperature vent fields appears to necessitate a magma lens undergoing continual replenishment, at least at intermediate spreading rates and higher [Baker, 2009; Lowell et al., 2013]. Magma-rich segments may be morphologically expressed as a relatively inflated bathymetric cross section [Scheirer and Macdonald, 1993], so cross-axis inflation (A_{xs}) may also be correlated with the spatial density of vent sites. Assessing the importance of factors such as magma budget to venting is made simpler by studying segments at a constant spreading rate, but the length of ridge crest examined in any single study governs the robustness of this approach. Detailed hydrothermal studies have never exceeded ~1000 continuous km of ridge crest [e.g., Baker and German, 2004].

Here we combine an earlier hydrothermal survey of the intermediate spreading rate Southeast Indian Ridge (SEIR), mainly focused on the Amsterdam-St. Paul (ASP) “hot spot” (i.e., a thermal or magmatic anomaly without regard to origin) [Scheirer et al., 1998], with new sampling along 19 first and second-order segments east of the hot spot. (Following Macdonald et al. [1991], first-order boundaries are transform faults and second-order boundaries are smaller, nontransform offsets with an off-axis trace.) These surveys total 227 stations along ~2500 km of ridge length, or ~4% of the total mid-ocean ridge (MOR). The data allow us to

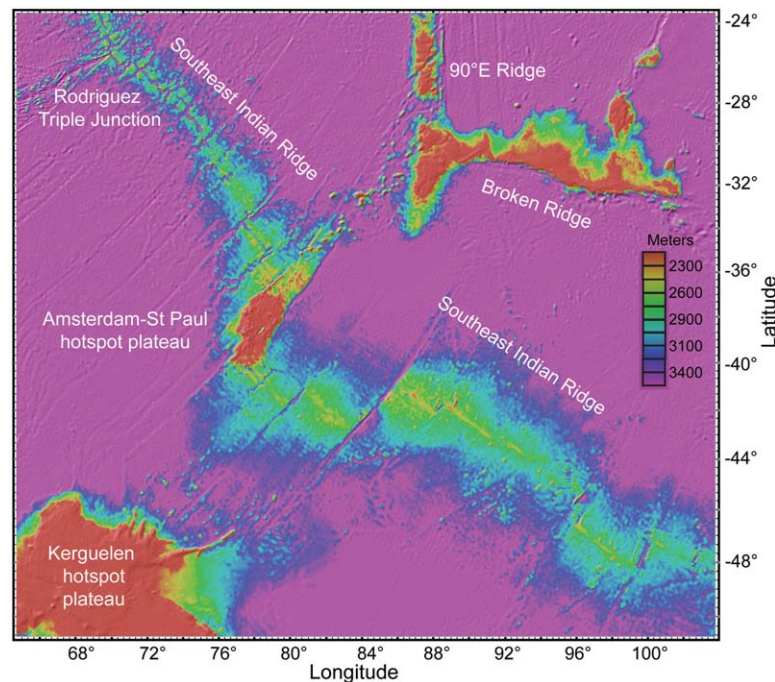


Figure 1. Regional bathymetry and principal features surrounding the Amsterdam-St. Paul hot spot plateau. This map and Figure 2 generated by GeoMapApp (<http://www.geomapapp.org>), topography from Ryan *et al.* [2009].

address two hypotheses. First, hydrothermal venting, or at least high-temperature venting, is significantly diminished along submarine MOR sections impacted by a hot spot. This effect has been noted on other ridges [Dyment *et al.*, 2007], but in each study sampling was restricted to ridge segments hundreds of km distant from the locus of the hot spot itself (Iceland [German *et al.*, 1994], Galápagos [Baker *et al.*, 2008], and Circe/Ascension [Devey *et al.*, 2005]). Second, hydrothermal venting is favored on ridge segments where morphology (depth, A_{xs}) or crustal properties (gravity anomalies) imply an

increased magmatic budget. This hypothesis also has been tested [Baker, 1996; Hooft *et al.*, 1997; Baker *et al.*, 2001], but never over a ridge crest section as long and as morphologically varied as our study area.

2. Geological Setting

Our study area lies just southeast of the Rodriguez Triple Junction (Figure 1). The regional geology has been summarized by Scheirer *et al.* [2000] and Conder *et al.* [2000] near the ASP hot spot and Cochran *et al.* [1997] east of 88°E. We adopt the segmentation labeling as originated by Royer and Schlich [1988] and Cochran *et al.* [1997], plus higher-resolution segmentation made visible by our bathymetric surveys [Brais *et al.*, 2011]. The SEIR around and bisecting the ASP hot spot is an intermediate rate ridge spreading at 65 mm/yr in the west to 71 mm/yr in the east [Ma and Cochran, 1996]. In the survey region the SEIR comprises 27 spreading segments ranging in length from ~30 to 200 km, totaling ~2500 km of axial length (Figure 2). Of the 28 segment boundaries along this section of the SEIR, 12 are transform faults, thus creating a relatively high frequency of first-order ridge segments.

Near the western end of our study area, the ASP hot spot has built a plateau that extends >400 km along the SEIR axis and is elevated as much as 1.5 km above the surrounding ridge axes [Scheirer *et al.*, 2000; Maia *et al.*, 2011]. Four segments (I1, I2, J1, and most of J2) run through the plateau, and a fifth (H) meets a geochemical definition of the hot spot (e.g., high R/R_A (the ratio of $^3\text{He}/^4\text{He}$ in rocks to that in air) [Graham *et al.*, 1999]). These segments are relatively short with significant overlaps. Cross-axis morphology ranges from axial valleys to rifted axial highs. Segments adjacent to the ASP Plateau (G, J3) feature axial valleys a few kilometers wide and several 100 m deep.

Farther east, the ridge becomes morphologically diverse. J4 begins as an axial valley but within a short distance becomes an axial high with a near-rectangular central graben some 200 m deep. K is a rifted axial high with four subsegments defined by individual bathymetric minima. L2 is a broad, unrifted volcanic high bracketed by two narrow axial highs often with a narrow graben 100–250 m deep (L1, L3). Segment M begins a large-scale axial deepening with two short subsegments (M1–2) containing another broad volcanic high that narrows and deepens into a rifted axial high (M3) ending in a prominent overlapping spreading

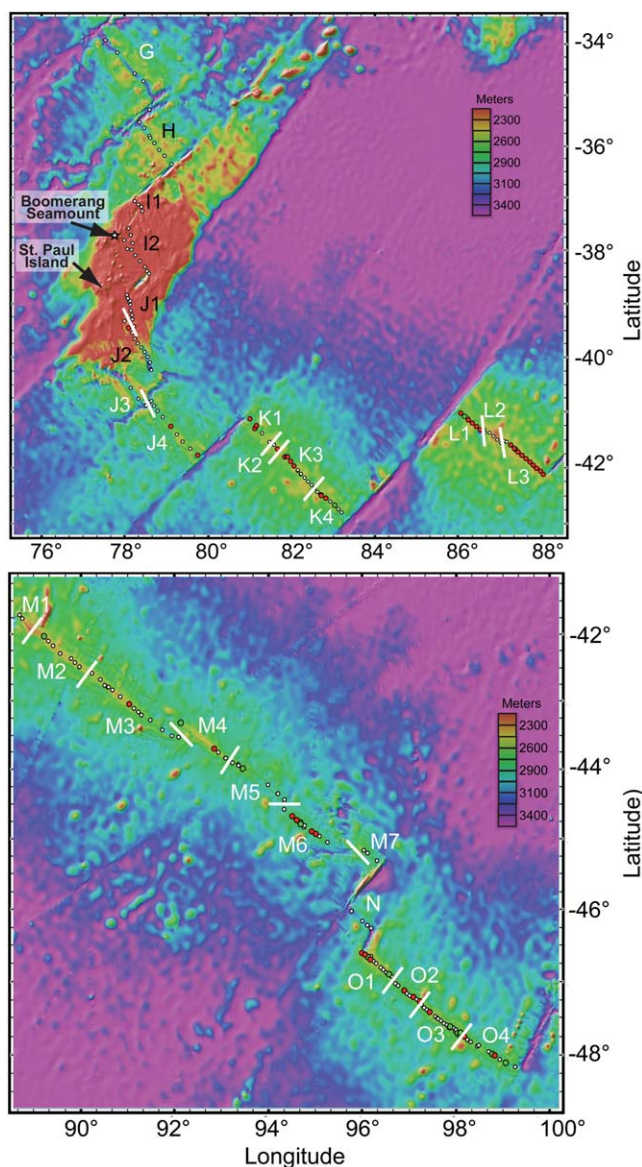


Figure 2. Bathymetry (color scale as in Figure 1) and ridge segmentation along the Southeast Indian Ridge in the study area. Segment boundaries are first order (letters only) except where marked by a white solid line (second order, numbered letters). Black lettering indicates segments on the ASP Plateau (bathymetric and/or chemical anomaly). Circles identify MAPR locations: white, no plume; red, definite hydrothermal plume; green, possible plume. Boomerang Seamount is considered the active expression of the ASP hot spot [Johnson et al., 2000].

2009/2010, also revisiting some of the 1996 sites. Station spacing varied from <1 to 71 km, with a mean of 11.3 km and a median of 9.9 km.

All Boomerang and GEISEIR profiles were collected by Miniature Autonomous Plume Recorders (MAPRs) attached to the wire on rock cores or dredges. MAPRs were attached to a conductivity-temperature-depth package during DY115-19. The typical nearest seafloor approach of the MAPRs on all vertical profiles was ~25 m. MAPRs are self-contained units that every 5 s (every 5 m at the standard vertical wire rate of 1 m/s) measured pressure, light backscatter, temperature, and, in 2010 only, oxidation-reduction potential (ORP; sometimes referred to as Eh). The voltage output of the light-backscatter sensors is equivalent to nephelometric turbidity units (NTU) [American Public Health Association, 1985]; ΔNTU is the value in excess of ambient water. ORP is highly sensitive to short-lived reduced chemicals in hydrothermal plumes, such as Fe⁺²,

center. Segment M4 is a narrow axial high that grades into the deeply rifted (~200 m) M5 segment. M6 and M7 are defined by distinct overlapping spreading centers. M6 has another narrow axial high at its center and M7 is a rifted axial high. N is a first-order segment with a wide axial valley as much as 600 m deep. O begins with the broad dome of O1 deepening into a narrow axial high (O2). O3 is another volcanic high, and O4 ends the segment as a broad axial valley with multiple axial volcanic ridges.

The larger Kerguelen hot spot, ~1400 km southwest of the ASP hot spot (Figure 1), has been suspected of influencing the depth of the SEIR axis east of the ASP Plateau [Small, 1995], but isotopic evidence from SEIR lavas only weakly supports this hypothesis [Mahoney et al., 2002; Nicolaysen et al., 2007].

3. Methods

Our data set of 227 water column profiles from 27 first and second-order ridge segments on and adjacent to the ASP Plateau extends for ~2500 km (Figure 2). Data were collected on four cruises from 1996 to 2010. The U.S. Boomerang cruise in 1996 collected 75 water column profiles on segments F to L [Scheirer et al., 1998] with dense coverage (51 stations) on the ASP Plateau and sparse coverage (24 stations) on the adjacent segments. The Chinese cruise DY115-19 reoccupied two of the Boomerang stations in 2007 [Wang et al., 2011]. The French GEISEIR project collected 150 profiles on segments K to O in

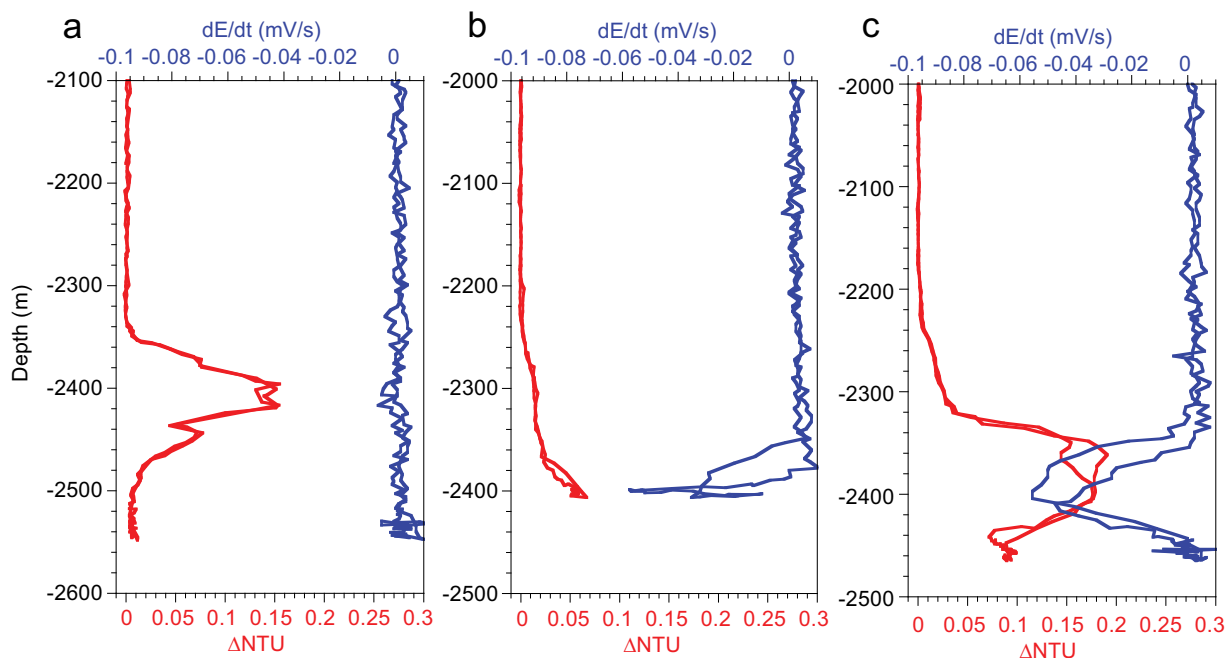


Figure 3. Typical MAPR profiles showing light backscatter anomaly as ΔNTU (red) and oxidation-reduction potential as the time derivative of the ORP value (dE/dt (mV/s); blue). Vertical and horizontal scales identical for each plot. (a) A plume with high ΔNTU but very weak dE/dt indicates an obvious plume from a source $> \sim 1$ km distant. (b) Near-bottom plume with both ΔNTU and dE/dt anomalies implies a nearby source with a low buoyancy flux. (c) An above bottom plume with both ΔNTU and dE/dt imply a nearby source with a higher buoyancy flux.

H_2S , and H_2 [Walker *et al.*, 2007]. Field experience shows that ORP anomalies are rarely found farther than ~ 1 km from their hydrothermal source [e.g., German *et al.*, 2008; Baker *et al.*, 2010]. Absolute values of the ORP sensor (E , mV) can vary because of instrumental drift and hysteresis, especially in concentrated plumes, so we rely on the time derivative, dE/dt , to identify the relative strength of anomalies. Because E declines when it encounters reduced substances, the anomalies are negative. Figure 3 shows examples of plume profiles.

Following Scheirer *et al.* [1998], we define plume incidence (p_h) as the fraction of the profiles exhibiting definite or possible evidence for a hydrothermal plume. Conceptually, the vertical profiles constitute a sample set from a continuous plume distribution. This definition is appropriate here because the stations are spaced approximately regularly along the segments (mean separation = 11.3 ± 9.2 km). To demonstrate that a sampling bias does not affect our p_h calculations, a plot of sample density in each segment versus p_h for both definite and possible plumes confirms that p_h is not correlated with sample density (Figure 4).

We calculated A_{xs} after the method of Scheirer and Macdonald [1993], with respect to a reference depth of 2800 m, for profiles 10 km long on either side of the axis in the spreading direction. We first combined high-resolution bathymetry data sets in the area with the bathymetry predicted from satellite altimetry [Smith and Sandwell, 1997] to obtain a bathymetry grid with no gaps. To remove any off-axis seamounts from the calculation of A_{xs} , we calculated the bathymetry anomaly with respect to the Stein and Stein [1994] model of lithospheric cooling, removed all features higher than 400 m in the anomaly grid, and combined the resulting grid with the cooling model to create a bathymetry grid with no large off-axis reliefs. The resulting grid was smoothed with a 1 km median filter. We extracted the 20 km long profiles from the smoothed bathymetry and calculated the area above the 2800 m reference level. For most segments, the 2800 m depth corresponds to an age of ~ 1 Myr. Negative values of A_{xs} reflect sections of the axis with an average depth along the cross-axis profiles deeper than 2800 m. Values were calculated every 1 km along axis. High-resolution bathymetry for this calculation is only available for those segments mapped in 2009

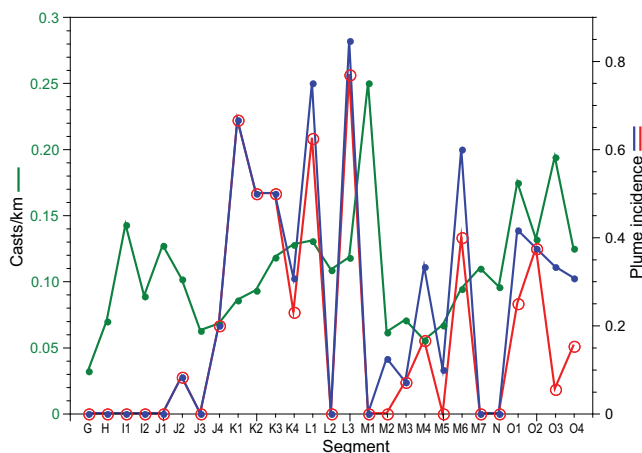


Figure 4. Comparison of the casts/km in each segment (green line) to the plume incidence for each segment considering only definite plumes (red line) or combined definite and possible plumes (blue line). First-order segments (letters only) are used where second-order segmentation is absent or undetermined. Data density along the ridge is not correlated with plume incidence.

and 2010 (K through O). A_{xs} for segments G, J3, and J4 were calculated in the same manner but only where earlier high-resolution bathymetry extended sufficiently far off-axis, typically ~ 6 profiles/segment.

Mantle Bouguer anomalies (MBA) were calculated using the available multibeam bathymetry grids and a merged grid composed of shipborne gravity measurements and satellite-derived free-air anomalies [Sandwell and Smith, 2009]. The model used for the calculations assumed constant crustal and mantle densities, respectively,

2800 and 3300 kg/m³, and a constant crustal thickness of 6 km. These parameters are slightly different from those used by Scheirer *et al.* [2000], who chose a two-layer crustal model. The differences between the MBA calculated with a two-layer model with densities of 2700 kg/m³ for a 2 km thick upper crust and 2900 kg/m³ for a 4 km thick lower crust and that calculated with the average crustal model used here are under 2 mGal and do not invalidate the use of Scheirer *et al.* [2000] results in our paper. The MBA lows denote areas of thicker crust compared to the model, or hotter (less dense) underlying mantle, and the MBA highs reveal zones of thinner crust, or colder (denser) mantle. The method of calculation is developed in Maia and Arkani-Hamed [2002].

Scheirer *et al.* [2000] and Maia *et al.* [2011] discussed the large MBA anomaly observed near the ASP Plateau, which is related to the thick crust produced by the interaction between the hot spot and the SEIR. We use the local, segment-scale MBA lows to confirm an abundant magma supply and the possibility of magma lenses at the non-ASP Plateau segments.

4. Regional Plume Distribution and the Hot Spot Effect

Twenty-one hot spot features occur directly beneath or close to a MOR [Dyment *et al.*, 2007] and cause physical and chemical anomalies along 20% of the global MOR [Ito *et al.*, 2003]. Regardless of their origin, they supply additional melt to the MOR, and so might increase hydrothermal activity. Surveys of some ridge sections close to a hot spot, however, have found less hydrothermal activity than on “normal” MORs of the same spreading rate. This association remains speculative because most hot spots are several hundred kilometers from a MOR, and few MOR segments near a hot spot have been surveyed in detail for hydrothermal activity.

In addition to this study, hydrothermal surveys have been conducted along four other ridge sections unquestionably or possibly affected by nearby hot spot activity: Reykjanes Ridge, 57°N–63°N (Iceland); Galápagos Spreading Center, 89.5°W–95°W (Galápagos); Mid-Atlantic Ridge, 7°S–12°S (Circe/Ascension); and Juan de Fuca Ridge, 45.5°N–46.5°N (Cobb). There are many indices that have been used to identify hot spot influence on ridge segments, but we focus on two prominent and widely used ones: bathymetric and R/R_A anomalies (Figure 5).

Along the slow spreading (20 mm/yr) Reykjanes Ridge from 57°45'N to 63°9'N, the ridge crest is an inflated axial high and lavas show mantle plume anomalies in R/R_A for at least 1000 km south of Iceland [Schilling, 1973; Poreda *et al.*, 1986]. German *et al.* [1994] found only a single vent site along 750 km of ridge. The Galápagos hot spot inflates the axial bathymetry and creates a slight but consistent R/R_A anomaly on the Galápagos Spreading Center from 91°W–93°W [Detrick *et al.*, 2002]. The p_h value is 0.09 for that ridge

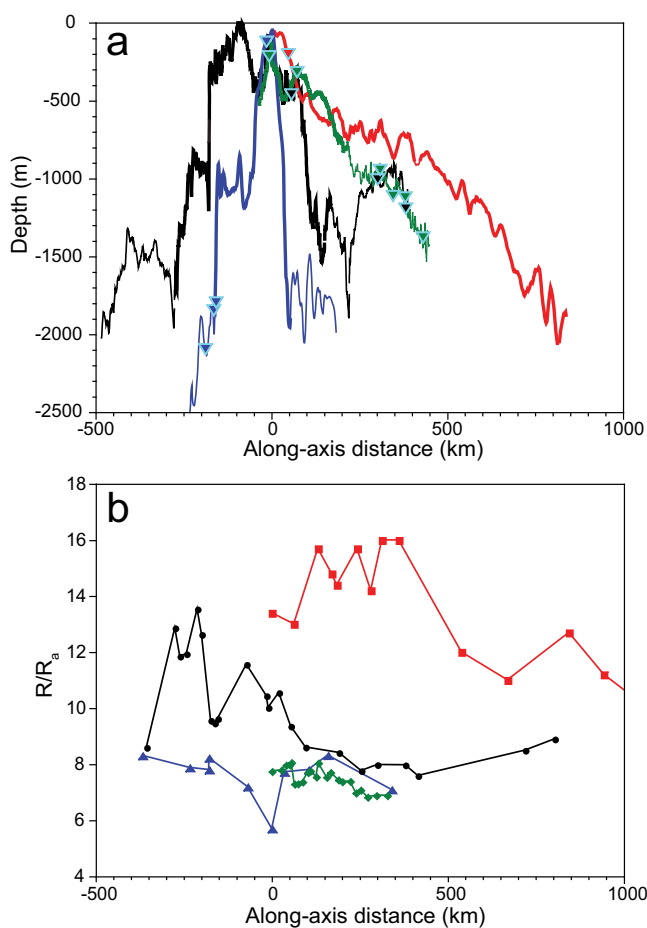


Figure 5. Along-axis anomalies in (a) bathymetry (data sources are this study, *Baker et al.* [2008] for Galapagos Spreading Center, and GeoMapApp [*Ryan et al.*, 2009] for Reykjanes Ridge and the Mid-Atlantic Ridge 7°S–12°S) and (b) R/R_A (data sources given in the text) for four ridge sections affected by hot spots. The y axis is centered on the bathymetric high point for each anomaly. In both figures, black lines and symbols are this study, red is the Reykjanes Ridge 57°N–63°N, green is the Galapagos Spreading Center 91°W–93°W, and blue is the Mid-Atlantic Ridge 7°S–12°S. In Figure 5a, heavy lines indicate the anomalous ridge sections, each normalized to 0 m depth at the shallowest point, and inverted triangles mark the location of known vent sites according to the InterRidge database (<http://www.interridge.org/IRvents>). R/R_A values for normal ridge basalts typically range between 7 and 9. The R/R_A and/or bathymetric anomalies occur over some 1850 km among these ridges, but include only five high-temperature vents. The other nine vents shown occur outside the anomaly regions.

Expedition, 1985; *ASHES Expedition*, 1986], analogous to that on Boomerang Seamount on the ASP Plateau, but in other respects the Cobb–Juan de Fuca interaction is an unsuitable comparison to other ridge–hot spot pairs.

The ASP Plateau is a rare example of a hot spot plateau bisected by a MOR. The most likely current expression of the hot spot, the hydrothermally active Boomerang Seamount, lies ~25 km from the nearest SEIR segment [*Johnson et al.*, 2000]. *Scheirer et al.* [1998] first noted the influence of the ASP Plateau on the regional distribution of hydrothermal plumes. They found that MOR segments crossing the plateau were nearly devoid of plumes. Along the spreading center axes, a single hydrothermal plume was observed on J2 at the southeastern edge of the plateau in the center of a clearly defined axial valley ~3 km wide with 100–200 m high walls. J2 is a propagating rift that begins on the ASP Plateau but ends ~1000 m deeper off the plateau [*Conder et al.*, 2000]. The one plume signal, however, is close to the plateau end of the segment. The near absence of plume signals on the plateau MOR occurs even in the face of recent volcanism at the northern end of I2 (near Boomerang Seamount), and the recent

section, compared to an expected value of 0.22 for a “normal” ridge spreading at the same rate [*Dyment et al.*, 2007]. Although the Circe/Ascension hot spot is weak or intermittent and its location uncertain [*Adam et al.*, 2007], it appears to have inflated a 200 km long section of the Mid-Atlantic Ridge between ~8°30’S and 10°30’S [*Minshull et al.*, 1998]. However, there is no clear R/R_A anomaly [*Graham et al.*, 1992] and only a single vent site has been located on the 200 km long inflated ridge section [*Devey et al.*, 2005]. The Cobb hot spot is bisected by the Juan de Fuca Ridge but otherwise is quite different than the hot spots described above. The Cobb-affected ridge segment has no R/R_A [*Lupton et al.*, 1993] or other isotopic [*Desonie and Duncan*, 1990] anomalies, and the bathymetric anomaly is the 700 m high on-axis Axial Volcano that extends along only a single, 100 km long ridge segment [*West et al.*, 2003] (cf. Figure 5). Because of voluminous lava flows there is no morphological expression of the spreading axis on the north or south flank of Axial Volcano. Known hydrothermal activity occurs only at the summit of Axial Volcano [*Canadian American Seamount*

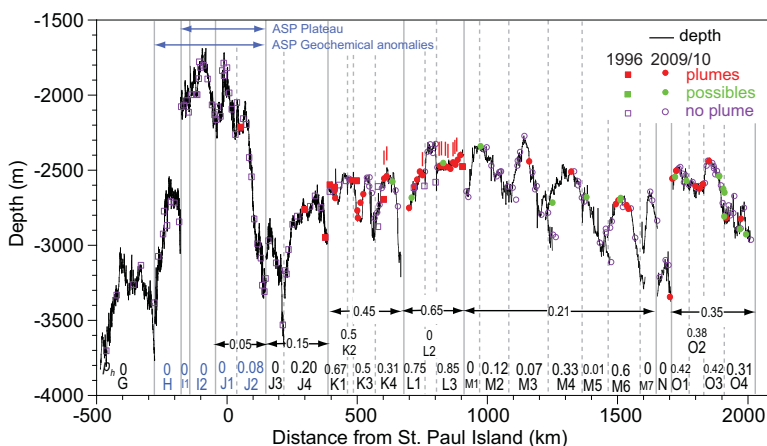


Figure 6. Bathymetry of the SEIR relative to the along-axis distance from St. Paul Island (see Figure 2). Symbols indicate station locations and distribution of observed hydrothermal plumes in 1996 (squares) and 2009 and 2010 (circles). Vertical red lines over K and L mark locations of ORP anomalies. Blue arrows at top show the bathymetric and geochemical extents of the ASP Plateau. Plume incidence and name of each segment given along bottom. Segment boundaries are solid gray lines for first order and dashed gray lines for second order. Double-headed arrows show plume incidence for entire first-order segments. The single plume over N was >1000 m above the local seafloor, indicating a probable origin on segment O.

relocation of ASP segments that may make them more effective conduits for hot spot-derived melts [Conder *et al.*, 2000].

In sharp contrast, seven stations occupied by Scheirer *et al.* [1998] on the sparsely sampled J3, J4, K, and L segments showed plume evidence. Combining the 1996 data from segments G, J3, J4, K, and L with our new sampling along segments K–O confirms and strengthens this distinction. We found definite evidence for hydrothermal plumes at 46 stations and possible evidence at 17 additional non-ASP Plateau stations (Figure 6). The overall p_h for all segments is 0.28 (63 of 227 stations), unevenly distributed as 0.02 for ASP Plateau segments and 0.34 for non-ASP Plateau segments. These results are further support for both the existing global trend of p_h versus spreading rate and the dampening of hydrothermal activity by hot spot construction (Figure 7). Of all submarine hot spot–MOR interactions surveyed, the ASP Plateau has by far the most reduced level of plume observations relative to its spreading rate or magmatic budget.

Haymon *et al.* [2008] offered three hypotheses for reduced abundance of hydrothermal vents along submarine ridge/hot spot interactions: reduced convective cooling due to elevated crustal temperatures creating a weak lithosphere, increased low-temperature cooling, and episodic hydrothermal activity. Hypothesis 1 cannot be addressed directly without information on the depth of any melt lenses present on the ASP Plateau (reduced cooling should lead to shallower lenses, as implied along the Reykjanes Ridge [Chen, 2003]). However, the abundance of melt near hot spots may imply that less fractures and faults develop between eruptions, preventing or shallowing the deep circulation of water, and therefore the convective cooling. Compiling the distribution and frequency of small earthquakes in the area, which should be lower near hot spots, might indirectly test the hypothesis. However, a 7 month long hydroacoustic monitoring of the SEIR from 72°E to 90°E found no obvious difference between earthquake distributions on and off the ASP Plateau [Hanson and Bowman, 2006]. Another possible cause for reduced convective flow is that, because of the large crustal thickness in hot spot-affected MOR, the melt lenses remain deeper than on normal MOR sections. These larger depths possibly prevent seawater from reaching the melt lenses, thus reducing hydrothermal flow.

We observed no instances of weak, near-bottom plumes at ASP Plateau sampling locations that would have favored hypothesis 2, but discrete sampling (as opposed to continuous tows) and the absence of an ORP sensor (sensitive to low-temperature plumes) made for poor testing of that hypothesis. Based on a set of bottom camera tows along the Galápagos Spreading Center, Haymon *et al.* [2008] argued for hypothesis 3: that consistency in the geologic setting, maturity, and deposit size of present-day vent sites suggests episodic magma delivery. Similar data for the ASP Plateau remain absent. Although we cannot make progress on determining the cause of reduced high-temperature (at least) venting at submarine ridge–hot spot intersections, our results demonstrate that the ASP Plateau is a prime candidate to test these hypotheses.

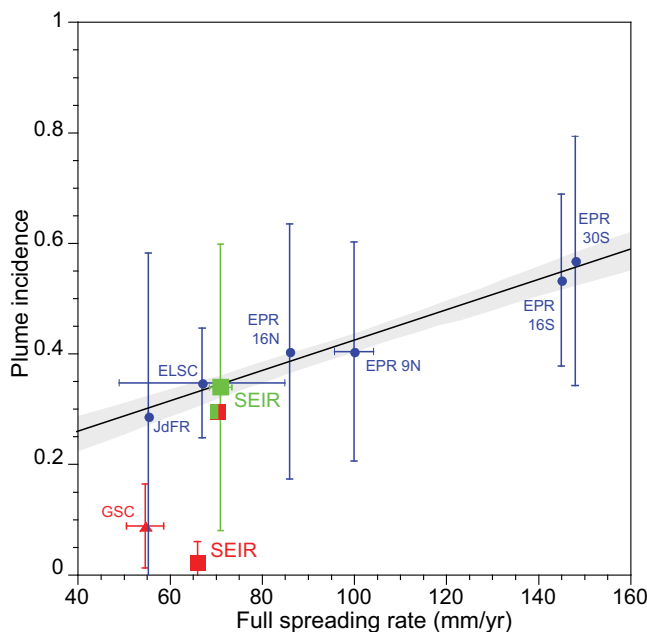


Figure 7. Scatterplot of plume incidence (p_h) versus spreading rate (u_s) for intermediate-rate to superfast-rate ridge sections. Error bars of ± 1 standard deviation are shown where they extend beyond the symbol. Standard deviation for plume incidence is derived from the variability of p_h among the segments of each section. Green square is the SEIR not influenced by the ASP hot spot, red square is the hot spot-affected SEIR and green/red box is the SEIR section point for all segments (not included in the regression). Blue dots are all other nonhot spot-affected sections and red triangle is the hot spot-affected Galápagos section (91°W – 93°W). Solid black line is the least squares regression fit to all nonhot spot ridge sections, gray band is the 95% confidence band for the slope ($p_h = 0.15 + 0.0027u_s$, $r = 0.99$, significant at the 5% level, $r_{(0.05,5)} = 0.67$). EPR is East Pacific Ridge, JdFR is Juan de Fuca Ridge, ELSC is Eastern Lau Spreading Center, and GSC is Galápagos Spreading Center. Non-SEIR data from Baker [1996] (JdFR, EPR 9°N – $11^\circ 48'\text{N}$, and EPR $13^\circ 30'\text{S}$ – 19°S), Baker et al. [2001] (EPR $15^\circ 15'\text{N}$ – $18^\circ 30'\text{N}$), Baker et al. [2002] (EPR $27^\circ 30'\text{S}$ – $32^\circ 18'\text{S}$), Martinez et al. [2006] (ELSC $19^\circ 20'\text{S}$ – $22^\circ 40'\text{S}$), and Baker et al. [2008] (GSC).

5. Segment-Scale Plume Distributions

5.1. First and Second-Order Segment Trends

Our second hypothesis is that hydrothermal venting is favored on ridge segments where morphology (depth, A_{xs}) or crustal properties (as expressed by the gravity field) imply an increased magmatic budget. We here test this hypothesis for the non-ASP Plateau segments at a variety of segment scales. We did not attempt to calculate A_{xs} values for the ASP Plateau segments because the rugged cross-axis bathymetry makes identification of a valid reference depth unreliable.

A glance at the distribution of observed plumes along the ridge axis shows that A_{xs} is uncorrelated with the occurrence of hydrothermal activity both within and among second-order segments (Figures 6 and 8). Within segments J4 to L3 and O1-4, plumes occur at both peaks

and valleys of depth and A_{xs} . Only along segment M, where hydrothermal plumes are sparse, do plumes predominantly occur where the axis is shallowest and most inflated. This difference may be related to intra-segment morphological variability. Only M is organized into a regular series of symmetrical along-axis highs, in both A_{xs} and depth, separated by distinct lows.

Segment L illustrates the striking variability possible among second-order segments. Segments L1 and L3 have the two highest p_h values in the study area but are separated by an even shallower and more inflated segment that was devoid of hydrothermal plumes. Segment L2 is an unusually broad and unrifted high that appears to have experienced a recent volcanic eruption. It is similar to the 16°N segment on the East Pacific Rise (EPR). That segment is the most inflated on the northern EPR, yet the p_h is unusually low (0.19) for a fast spreading ridge, perhaps because rifting has not yet fractured the volcanic carapace from a recent eruption, or because a local excess of magma prevents faulting and fracturing, therefore lowering the water recharge for hydrothermal circulation [Baker et al., 2001].

We test the value of A_{xs} as a predictor of hydrothermal activity on second-order segments by examining the correlation between A_{xs} and p_h . Baker [1996] found a good correlation ($r = 0.71$) significant even at the 1% level ($r_{(0.01,17)} = 0.575$) based on 14 second to fourth-order segments from superfast to intermediate spreading rates. The SEIR data are a good test of this correlation, because at a near-uniform spreading rate they span almost the entire global range of published A_{xs} versus p_h data. For the 20 non-ASP Plateau second-order SEIR segments, a least squares fit shows a weak correlation ($p_h = 0.20 + 0.048A_{xs}$, $r = 0.38$) that is non-significant at the 5% level ($r_{(0.05,18)} = 0.444$). Moreover, the predictive value of this fit is low, with an A_{xs} intercept of $p_h = 0.20$, implying substantial venting even with no magmatic inflation.

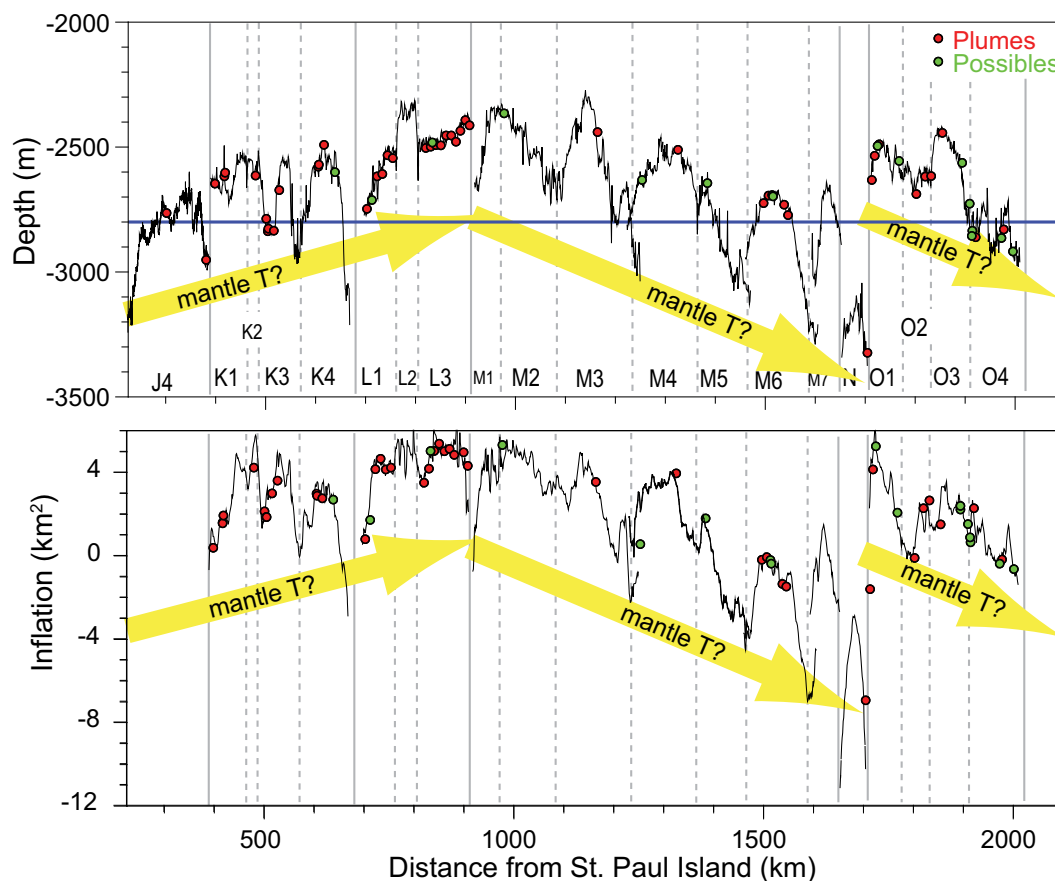


Figure 8. Comparison of along-axis trends in both bathymetry and cross-axis inflation. Yellow arrows show multisegment trends in both indices, which may correspond to trends in mantle temperature. The shallowing depth trend of segments J4 through L3 is the easternmost portion of a trend that begins at least as far back as segment G [Scheirer *et al.*, 2000]. Blue line indicates the reference depth for cross-axis inflation calculations. Segment boundaries demarcated as in Figure 6.

We next add the SEIR results to other second-order segments using the A_{xs} and p_h data from Baker [1996] and additional newer data from 15°N–18°N [Baker *et al.*, 2001] and 27°30'S–32°20'S [Baker *et al.*, 2002] on the EPR. For 37 second-order segments (median length 96 km), the linear fit of A_{xs} versus p_h is almost identical to that from the SEIR segments alone ($p_h = 0.20 + 0.064A_{xs}$), but with a slightly higher ($r = 0.48$) and significant ($r_{(0.05,35)} = 0.325$) correlation (Figure 9a). Newer data thus suggest that the results of Baker [1996] were too optimistic. Even though A_{xs} and p_h are weakly correlated, A_{xs} is clearly a poor predictor of second-order segment p_h . We conclude that second-order segments are not magmatically independent enough to maintain distinct A_{xs} versus p_h identities.

Because first-order segments are isolated by high-offset and long-lasting boundaries (transform faults or other large offsets), we expect a higher correlation between segment morphology and hydrothermal activity compared to second-order segments. Grouping the second-order segments from Figure 9a into first-order segments (median length 278 km), the least squares fit for A_{xs} versus p_h ($p_h = 0.25 + 0.063A_{xs}$) shows a significant correlation ($r = 0.85$; $r_{(0.05,12)} = 0.458$; Figure 9b). The result is geologically unproductive, however, because it predicts a robust p_h value (0.25) for $A_{xs} = 0$. This results from the inclusion of two segments with $A_{xs} \ll 0$. Although it is geologically reasonable to expect p_h to increase as the magma supply (A_{xs}) increases from zero, all negative A_{xs} values imply a state of no or minimal magma supply. Excluding segments where $A_{xs} < 0$ leaves the correlation essentially unchanged ($p_h = 0.07 + 0.12A_{xs}$, $r = 0.85$; $r_{(0.05,10)} = 0.497$) and significantly lowers the A_{xs} intercept value from $p_h = 0.25$ to 0.07. The data thus show that A_{xs} is an excellent predictor of p_h for first-order segments with $A_{xs} \geq 0$, a geologically satisfying conclusion.

Segment-scale data tell us where activity is likely, but not the precise location of vent fields. Because fine-grained hydrothermal precipitates can be advected many kilometers along axis, vertical profiles of ΔNTU

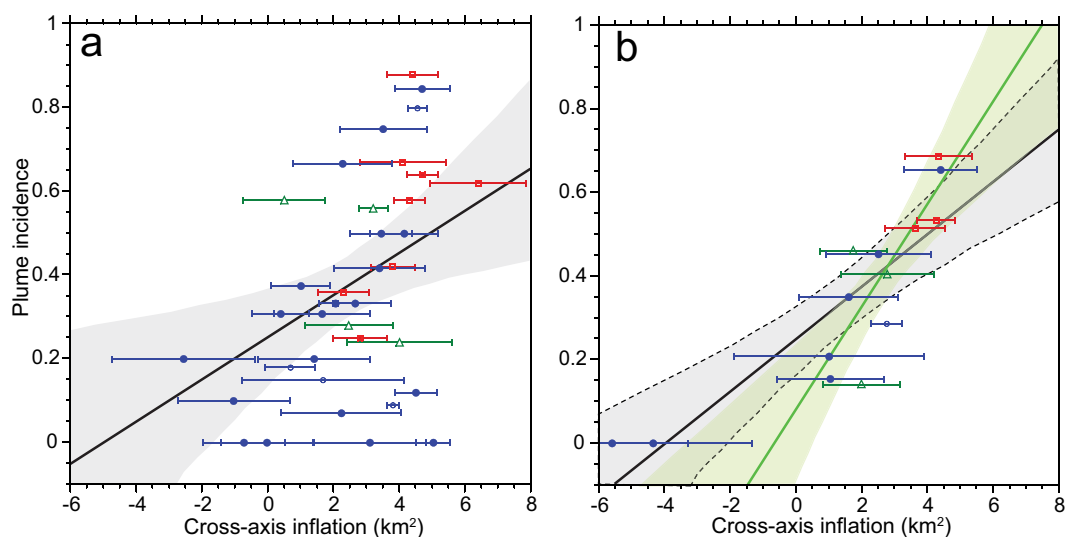


Figure 9. Scatterplots of plume incidence (p_h) versus cross-axis inflation (A_{xs}). (a) Individual second-order segments for intermediate to superfast rate ridge segments. Symbol color key is blue, intermediate rate; green, fast rate; and red, superfast rate. Large solid symbols are from the SEIR (not including ASP Plateau segments). Black line shows the least squares fit to all segments ($p_h = 0.20 + 0.064A_{xs}$, $r = 0.48$). Gray band is the 95% confidence interval for the slope. (b) Individual first-order segments from the same data set. Black line is the least squares fit to all segments ($p_h = 0.25 + 0.063A_{xs}$, $r = 0.85$); green line is the fit to all segments with inflation ≥ 0 ($p_h = 0.074 + 0.12A_{xs}$, $r = 0.85$). Gray and green bands are the 95% confidence bands for each fit. Non-SEIR data from Baker [1996], Baker et al. [2001], and Baker et al. [2002].

anomalies are not always a reliable indicator of the precise location of active vent fields. ORP anomalies, however, locate active sources to within ~ 1 km or less. ORP data are only available from the 2010 cruise to segments K and L, where distinct anomalies were detected at 10 separate locations (Figure 6). Segment L hosted most of the ORP anomalies, and would thus be a first choice for seafloor exploration along this part of the SEIR. Of nine ORP profiles along L3, seven had clear plume anomalies. Given a spacing of 7–10 km between each profile, each must have sampled a separate vent field or fields. This collection of active fields along 80 km of ridge axis is unusual even for superfast spreading ridges and unknown on intermediate rate ridges [e.g., Baker, 2009].

5.2. Multisegment Trends

Bathymetric trends define four major sections, and each has a distinct hydrothermal character. As noted above, the ASP Plateau is both the shallowest and most hydrothermally barren of the four sections. Individual cross-axis profiles clearly demonstrate that deep valleys (>200 m) are the hallmark of these segments. Given the positive correlation between A_{xs} and p_h for “normal” ridge segments (Figure 9), the preponderance of axial valleys is consistent with the observed lack of plumes.

The non-ASP segments can be grouped into three sections distinguished by the along-axis trends in bathymetry and inflation (Figure 8). Along the westernmost section, non-ASP Plateau segments shallow and inflate from G thru L. A southeasterly increasing melt supply owing to higher mantle temperatures may contribute to this trend [e.g., Russo et al., 2009]. Plume incidence steadily increases along this gradient, from 0 at G and J3 to the regional max of 0.85 at L3.

The next section includes segments M and N, where the regional trend of axial depth and A_{xs} reverses and mean p_h falls to 0.2. Plumes on these segments are mostly found at or near peaks in axial depth and A_{xs} (though note the highly inflated portion of M4 was poorly sampled). The abruptness of the L-M transition is evidenced by the fact that M1–2 has a mean A_{xs} value (4.1 km^2) equal to L1 and L3 (4.2 km^2) but is almost devoid of plumes.

A prominent transition across the fracture zone between N and O defines the beginning of the easternmost section. Relative to M and N, axial depth sharply shallows, A_{xs} swells, and p_h increases to 0.35 on O (though the proportion of possible plumes is higher than on other segments) without regard to local peaks in axial

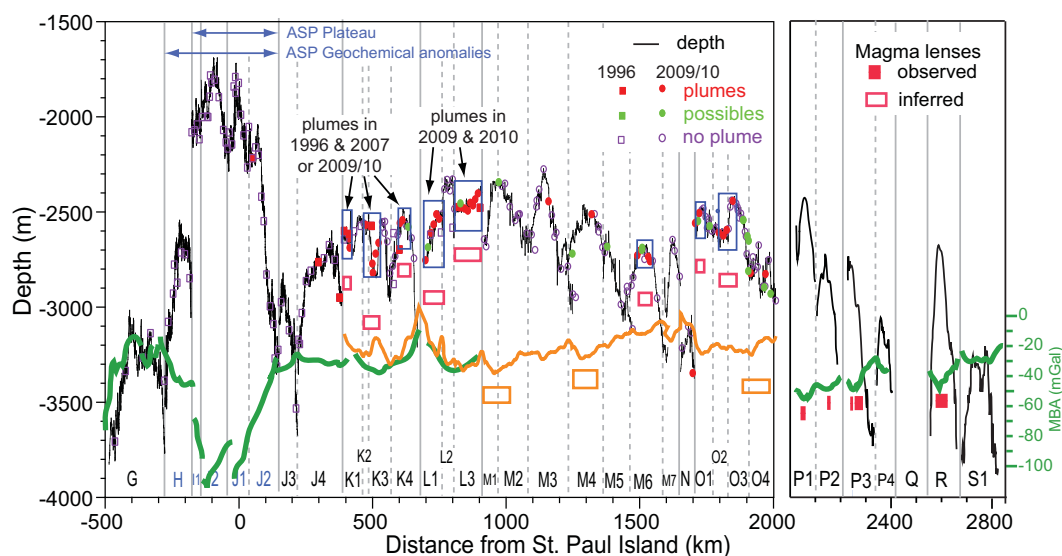


Figure 10. Along-axis data from this study compared to that of *Baran et al.* [2005] immediately east of our area (segments P1–S1). Heavy green lines are mantle Bouguer anomaly (MBA) from *Scheirer et al.* [2000] and *Baran et al.* [2005]. Heavy orange line is MBA from this study. Open blue boxes identify plume clusters. Solid red boxes show locations (but not depth) of AMC lenses observed by *Baran et al.* [2005]; open red boxes show minimum magma lens extents inferred from our plume observations; open orange boxes show supplementary lens extents inferred from our MBA profile, bathymetry, and nonclustered plumes. Segment boundaries demarcated as in Figure 6.

depth or A_{xs} . Segment O begins a long regional deepening of the SEIR that continues until the Australian–Antarctic Discordance near 126°E [*Ma and Cochran*, 1996].

Regional (multisegment) changes in ridge morphology along the SEIR are thought to be influenced by along-axis changes in mantle temperature, which mediates the rate of magma supply to the crust [*Cochran et al.*, 1997; *Sempère et al.*, 1997]. Our results suggest this interpretation can be extended to hydrothermal activity. On the regional scale, changes in p_h are greatest where the regional depth trend reverses (between L and M) and where the largest jump in axial depth and inflation occurs (between N and O). On a finer scale, *Baran et al.* [2005], working along the SEIR immediately east of our study area, found step-like transitions when comparing magma lens depth and layer 2A thickness to morphological changes (Figure 10). Magma lenses were imaged beneath second-order segments with an axial high but not those with axial valleys, and this distinction occurred even within some segments that were transitional between these extremes. *Baran et al.* [2005] attributed these transitions to local variations in magma supply. We see similar transitions on the first-order segment scale, with a strong correlation between A_{xs} and p_h (Figure 9b).

6. Implications for Melt Distribution Along the SEIR

A review of the six multisegment MOR sections where both hydrothermal plumes and axial magma lenses have been mapped found that detectable plumes and >90% of known vents occur exclusively over or immediately adjacent to the mapped locations of magma lenses, which extend over only ~50% of the total surveyed length (~2700 km) [*Baker*, 2009]. Thus magma, not simply “hot rock,” is necessary to support (at least) high-temperature venting. These observations imply that the distribution of hydrothermal activity can be used to estimate the minimum extent of magma expected along a ridge section.

In our study area, 85% of definite or possible plume stations occur in eight clusters (i.e., a group of stations where the median distance between each definite or possible plume is <11 km), which combine for a length of 350 km, or 17% of the non-ASP Plateau length (14% of the total ridge length; Figure 10). Five of the clusters have evidence for multiyear activity, as determined by observations 1–13 years apart (depending on location). We predict that these clusters define the minimum extent of magma lenses in the study area. Lenses may also lie beneath solitary plume sites at other locations, such as segments M1–2 and M4, where plumes occur at bathymetric highs and local lows in MBA are observed (Figure 10). A magma lens may also underlie segment O4, where several more widely separated plumes were found (though there is

no local low in MBA). Magma lenses under these segments could increase coverage by as much as ~ 300 km, doubling the non-ASP Plateau coverage to $\sim 30\%$. The true extent of magma lenses is almost certainly greater than our minimal 17% estimate because only lenses undergoing a period of replenishment are likely to sustain high-temperature venting [Lowell *et al.*, 2013].

Baran *et al.* [2005] provided a direct measure of the extent of magma lenses we might expect in our study area by surveying the SEIR immediately to the east (Figure 10). Of six segments totaling ~ 620 km, magma lenses were imaged along only four, covering 19% of the surveyed axis length, similar to our minimal estimate from plumes. These lenses occurred only where the cross-axis morphology was a simple axial high or a rifted axial high and corresponded to local lows in the MBA. However, a much broader extent of magma lenses has been mapped on other intermediate spreading ridges, such as the Juan de Fuca Ridge (60% of 380 km) [Carbotte *et al.*, 2006] and central Galápagos Spreading Center (68% of 380 km) [Detrick *et al.*, 2002], and on the intermediate to fast spreading Eastern Lau Spreading Center (55% of 500 km) [Jacobs *et al.*, 2007]. Despite extensive magma lenses on these ridges, both the Juan de Fuca Ridge and the Eastern Lau Spreading Center have a p_h value similar to the SEIR (Figure 7). Plume incidence on the Galápagos Spreading Center is lower, as are all surveyed hot spot-affected ridges.

Based on these results, the plume incidence data from our study are consistent with a true magma lens extent much longer than our minimal estimate of 17% for non-ASP Plateau segments. That Baran *et al.* [2005] found magma lenses on only 19% of the ridge might be a result of the regional change in axial morphology that occurs near 104°E , the boundary between P3 and P4 [Ma and Cochran, 1996; Baran *et al.*, 2005]. The ridge from the ASP Plateau to 104°E , except for the short segments J3 and N, is preponderantly an axial high. From 104°E to the Australia-Antarctic Discordance, however, all segments except for a single subsegment of R ($\sim 107^\circ 30'\text{E}$) are axial valleys. Thus, the ridge studied by Baran *et al.* [2005] marks the beginning of a long stretch of abnormally cool mantle, and presumably fewer opportunities for hydrothermal venting. Segments with axial highs in the Baran *et al.* [2005] region, P1-3, probably better represent our study area. They extend for 280 km, a 40% coverage, and host 90% of the observed magma lenses. This value is more consistent with results from our study (estimated 17%–30%) and other intermediate rate MORs.

7. Conclusions

The spatial density of hydrothermal plumes, p_h , and thus active vent sites, is variable at several scales related to the apparent magmatic budget along 2500 km of the axis of the Southeast Indian Ridge. The largest scale is four multisection sections that define major along-axis changes in long-term magma supply. The most prominent section is the Amsterdam-St. Paul hot spot plateau, which rises as much as ~ 1.5 km above the local bathymetry. Plumes are virtually absent ($p_h = 0.02$) from ridge segments that cross the plateau, consistent with hydrothermal surveys on other ridges affected by a hot spot. The mean p_h (0.34) from all nonhot spot segments is similar to other intermediate spreading ridges, but plumes are not evenly distributed. Plumes are most common on the section where seafloor depth shallows and cross-axis inflation increases to the east, a trend generally attributed to increasing magma supply and, perhaps, mantle temperature. Plumes are scarcer on the sections where depth increases and inflation decreases eastward.

We used data from this study and from five other surveyed ridge sections to test the correlation between cross-axis inflation and p_h at the segment scale. At the first-order segment scale, cross-axis inflation is a strong predictor ($r = 0.85$) of p_h , but we found only a weak and geologically unhelpful correlation ($r = 0.48$) at the second-order segment scale. These observations are consistent with the view that the relative inflation among first-order segments is a good estimate of local magma supply because of the strong and long-lasting barriers (usually transform faults) that separate them.

Eighty-five percent of plumes were grouped in eight clusters where the median distance between each plume was < 11 km. Five of the eight clusters occurred in the section with eastward shallowing depths and swelling cross-axis inflation. Because high-temperature venting on other ridge axes is almost exclusively associated with the presence of a magma lens, we hypothesize that the total cluster axial length of 350 km, 17% of the non-ASP axis, represents the minimum extent of axial magma lenses present. This estimate increases to $\sim 30\%$ if we include axis portions with multiple plumes, or with bathymetric highs and a corresponding local low in the MBA that host at least one plume.

Acknowledgments

J. Hein, R. Haymon, and two anonymous reviewers provided comments. We thank the Masters and crews of RV "Marion Dufresne II" and the engineers of IPEV for help during the GEISEIR I and II cruises and M. Clog for operating MAPRs during GEISEIR I. The GEISEIR project and cruise was funded by IPEV through the "Flotte Océanographique Française" and by CNRS-INSU through the "Campagnes à la mer" program. The 1996 cruise and subsequent work was funded by NSF grant OCE-9505667. Additional funding was supplied by the NOAA Vents (now Earth-Ocean Interactions) Program and the Joint Institute for the Study of the Atmosphere and Ocean (JISAO) under NOAA Cooperative Agreement NA10OAR4320148. PMEL contribution 4133, JISAO contribution 2207. Data for axial depth and location, the cross-axis inflation, the mantle Bouguer anomaly of the Southeastern Indian Ridge in our study area, and MAPR profile locations and statistics for plume spatial density in each segment can be found in Tables S1–S3 in the supporting information. MAPR profiles are available from PMEL by request to ETB or SLW.

References

- Adam, C., V. Vidal, and J. Escartin (2007), 80-Myr history of buoyancy and volcanic fluxes along the trails of the Walvis and St. Helena hotspots (South Atlantic), *Earth Planet. Sci. Lett.*, *261*, 432–442, doi:10.1016/j.epsl.2007.07.005.
- American Public Health Association (1985), *Standard Methods for the Examination of Water and Wastewater*, 16th ed., 1268 pp., Am. Publ. Health Assoc., Washington, D. C.
- ASHES Expedition (1986), Pisces submersible exploration of a high-temperature vent field in the caldera of Axial Volcano, Juan de Fuca Ridge, *Eos Trans. AGU*, *67*, 1027.
- Baker, E. T. (1996), Geological indexes of hydrothermal venting, *J. Geophys. Res.*, *101*, 13,741–13,753.
- Baker, E. T. (2009), Relationships between hydrothermal activity and axial magma chamber distribution, depth, and melt content, *Geochem. Geophys. Geosyst.*, *10*, Q06009, doi:10.1029/2009GC002424.
- Baker, E. T., and C. R. German (2004), On the global distribution of hydrothermal vent fields, in *Mid-Ocean Ridges: Hydrothermal Interactions Between the Lithosphere and Oceans*, *Geophys. Monogr. Ser.*, vol. 148, edited by C. R. German, J. Lin, and L. M. Parson, pp. 245–266, AGU, Washington, D. C.
- Baker, E. T., M.-H. Cormier, C. H. Langmuir, and K. Zavala (2001), Hydrothermal plumes along segments of contrasting magmatic influence, 15°20′–18°30′N, East Pacific Rise: Influence of axial faulting, *Geochem. Geophys. Geosyst.*, *2*(9), 1051, doi:10.1029/2000GC000165.
- Baker, E. T., et al. (2002), Hydrothermal venting along Earth's fastest spreading center: East Pacific Rise, 27.5°–32.3°, *J. Geophys. Res.*, *107*(B7), 2130, doi:10.1029/2001JB000651.
- Baker, E. T., R. M. Haymon, J. A. Resing, S. M. White, S. L. Walker, K. C. Macdonald, and K. Nakamura (2008), High-resolution surveys along the hot spot-affected Galápagos Spreading Center: 1. Distribution of hydrothermal activity, *Geochem. Geophys. Geosyst.*, *9*, Q09003, doi:10.1029/2008GC002028.
- Baker, E. T., F. Martinez, J. A. Resing, S. L. Walker, N. J. Buck, and M. H. Edwards (2010), Hydrothermal cooling along the Eastern Lau Spreading Center: No evidence for discharge beyond the neovolcanic zone, *Geochem. Geophys. Geosyst.*, *11*, Q08004, doi:10.1029/2010GC003106.
- Baran, J. M., J. R. Cochran, S. M. Carbotte, and M. R. Nedimović (2005), Variations in upper crustal structure due to variable mantle temperature along the Southeast Indian Ridge, *Geochem. Geophys. Geosyst.*, *6*, Q11002, doi:10.1029/2005GC000943.
- Briais, A., C. Hémond, M. Maia, B. B. Hanan, and D. W. Graham (2011), Tectonics at the Southeast Indian Ridge 79° to 99°E. Results from the GEISEIR cruises, Abstract T23D-2431 presented at 2011 Fall Meeting, AGU, San Francisco, Calif., 5–9 Dec.
- Canadian American Seamount Expedition (1985), Hydrothermal vents on an axis seamount of the Juan de Fuca Ridge, *Nature*, *313*, 212–214.
- Carbotte, S. M., R. S. Detrick, A. Harding, J. P. Canales, J. Babcock, G. Kent, E. Van Ark, M. Nedimovic, and J. Diebold (2006), Rift topography linked to magmatism at the intermediate spreading Juan de Fuca Ridge, *Geology*, *34*, 209–212, doi:10.1130/G21969.1.
- Chen, Y. J. (2003), Influence of the Iceland mantle plume on crustal accretion at the inflated Reykjanes Ridge: Magma lens and low hydrothermal activity?, *J. Geophys. Res.*, *108*(B11), 2524, doi:10.1029/2001JB000816.
- Cochran, J. R., J.-C. Sempere, and the SEIR Scientific Team (1997), The Southeast Indian Ridge between 88°E and 118°E: Gravity anomalies and crustal accretion at intermediate spreading rates, *J. Geophys. Res.*, *102*, 15,463–15,487.
- Conder, J. A., D. S. Scheirer, and D. W. Forsyth (2000), Seafloor spreading on the Amsterdam-St. Paul hotspot plateau, *J. Geophys. Res.*, *105*, 8263–8277.
- Desonie, D. L., and R. A. Duncan (1990), The Cobb-Eickelberg Seamount Chain: Hotspot volcanism with mid-ocean ridge basalt affinity, *J. Geophys. Res.*, *95*, 12,697–12,711, doi:10.1029/JB095iB08p12697.
- Detrick, R. S., J. M. Sinton, G. Ito, J. P. Canales, M. Behn, T. Blacic, B. Cushman, J. E. Dixon, D. W. Graham, and J. Mahoney (2002), Correlated geophysical, geochemical and volcanological manifestations of plume-ridge interaction along the Galápagos Spreading Center, *Geochem. Geophys. Geosyst.*, *3*(10), 8501, doi:10.1029/2002GC000350.
- Devey, C. W., K. S. Lackschewitz, and E. T. Baker (2005), Hydrothermal and volcanic activity found on the southern Mid-Atlantic Ridge, *Eos Trans. AGU*, *86*(22), 209–212.
- Dyment, J., J. Lin, and E. T. Baker (2007), Ridge-hotspot interactions—What mid-ocean ridges tell us about deep Earth processes, *Oceanography*, *20*, 102–115.
- German, C. R., et al. (1994), Hydrothermal activity on the Reykjanes Ridge: The Steinahóll Vent-field at 63°06′N, *Earth Planet. Sci. Lett.*, *121*, 647–654.
- German, C. R., D. R. Yoerger, M. Jakuba, T. M. Shank, C. H. Langmuir, and K. Nakamura (2008), Hydrothermal exploration with the Autonomous Benthic Explorer, *Deep Sea Res., Part 1*, *55*(2), 203–219.
- Graham, D. W., W. J. Jenkins, J.-G. Schilling, G. Thompson, M. D. Kurz, and S. E. Humphris (1992), Helium isotope geochemistry of mid-ocean ridge basalts from the South Atlantic, *Earth Planet. Sci. Lett.*, *110*, 133–147, doi:10.1016/0012-821X(92)90044-V.
- Graham, D. W., K. T. M. Johnson, L. D. Priebe, and J. E. Lupton (1999), Hotspot-ridge interaction along the Southeast Indian Ridge near Amsterdam and St. Paul islands: Helium isotope evidence, *Earth Planet. Sci. Lett.*, *167*, 297–310.
- Hanson, J. A., and J. R. Bowman (2006), Methods for monitoring hydroacoustic events using direct and reflected T waves in the Indian Ocean, *J. Geophys. Res.*, *111*, B02305, doi:10.1029/2004JB003609.
- Haymon, R., S. M. White, E. T. Baker, P. G. Anderson, K. C. Macdonald, and J. A. Resing (2008), High-resolution surveys along the hot spot-affected Galápagos Spreading Center: 3. Black smoker discoveries and the implications for geological controls on hydrothermal activity, *Geochem. Geophys. Geosyst.*, *9*, Q12006, doi:10.1029/2008GC002114.
- Hoof, E. E. E., R. S. Detrick, and G. M. Kent (1997), Seismic structure and indicators of magma budget along the southern East Pacific Rise, *J. Geophys. Res.*, *102*, 27,319–27,340.
- Ito, G., L. J. Lin, and D. Graham (2003), Observational and theoretical studies of the dynamics of mantle plume-mid-ocean ridge interaction, *Rev. Geophys.*, *41*(4), 1017, doi:10.1029/2002RG000117.
- Jacobs, A. M., A. J. Harding, and G. M. Kent (2007), Axial crustal structure of the Lau back-arc basin from velocity modeling of multichannel seismic data, *Earth Planet. Sci. Lett.*, *259*, 239–255, doi:10.1016/j.epsl.2007.04.021.
- Johnson, K. T. M., D. W. Graham, K. H. Rubin, K. Nicolaysen, D. S. Scheirer, D. W. Forsyth, E. T. Baker, and L. M. Douglas-Priebe (2000), Boomerang Seamount: The active expression of the Amsterdam-St. Paul hotspot, Southeast Indian Ridge, *Earth Planet. Sci. Lett.*, *183*, 245–259.
- Lowell, R. P., A. Farough, J. Hoover, and K. Cummings (2013), Characteristics of magma-driven hydrothermal systems at oceanic spreading centers, *Geochem. Geophys. Geosyst.*, *14*, 1756–1770, doi:10.1002/ggge.20109.
- Lupton, J. E., D. W. Graham, J. R. Delaney, and H. P. Johnson (1993), Helium isotope variations in Juan de Fuca Ridge basalts, *Geophys. Res. Lett.*, *20*, 1851–1854.

- Ma, Y., and J. R. Cochran (1996), Transitions in axial morphology along the Southeast Indian Ridge, *J. Geophys. Res.*, *101*, 15,849–15,866.
- Macdonald, K. C., D. S. Scheirer, and S. M. Carbotte (1991), Mid-ocean ridges: Discontinuities, segments, and giant cracks, *Science*, *253*, 986–994.
- Mahoney, J. J., D. W. Graham, D. M. Christie, K. T. M. Johnson, L. S. Hall, and D. L. Vonderhaar (2002), Between a hotspot and a cold spot: Isotopic variation in the Southeast Indian Ridge asthenosphere, 86°E–118°E, *J. Petrol.*, *43*, 1155–1176.
- Maia, M., and J. Arkani-Hamed (2002), The support mechanism of the young Foundation Seamounts inferred from bathymetry and gravity, *Geophys. J. Int.*, *149*, 190–210.
- Maia, M., et al. (2011), Building of the Amsterdam-Saint Paul plateau: A 10 Myr history of a ridge-hot spot interaction and variations in the strength of the hot spot source, *J. Geophys. Res.*, *116*, B09104, doi:10.1029/2010JB007768.
- Martinez, F., B. Taylor, E. T. Baker, J. A. Resing, and S. L. Walker (2006), Opposing trends in crustal thickness and spreading rate along the back-arc Eastern Lau Spreading Center: Implications for controls on ridge morphology, faulting, and hydrothermal activity, *Earth Planet. Sci. Lett.*, *245*, 655–672.
- Minshull, T. A., N. J. Bruguier, and J. M. Brozena (1998), Ridge-plume interactions or mantle heterogeneity near Ascension Island?, *Geology*, *26*, 115–118, doi:10.1130/0091-7613.
- Nicolaysen, K. P., F. A. Frey, J. J. Mahoney, K. T. M. Johnson, and D. W. Graham (2007), Influence of the Amsterdam/St. Paul hot spot along the Southeast Indian Ridge between 77° and 88°E: Correlations of Sr, Nd, Pb, and He isotopic variations with ridge segmentation, *Geochem. Geophys. Geosyst.*, *8*, Q09007, doi:10.1029/2006GC001540.
- Poreda, R., J.-G. Schilling, and H. Craig (1986), Helium and hydrogen isotopes in ocean-ridge basalts north and south of Iceland, *Earth Planet. Sci. Lett.*, *78*, 1–17.
- Royer, J. Y., and R. Schlich (1988), Southeast Indian Ridge between the Rodriguez Triple Junction and the Amsterdam and Saint-Paul Islands—Detailed kinematics for the past 20 My, *J. Geophys. Res.*, *93*, 13,524–13,550.
- Russo, C. J., K. H. Rubin, and D. W. Graham (2009), Mantle melting and magma supply to the Southeast Indian Ridge: The roles of lithology and melting conditions from U-series disequilibria, *Earth Planet. Sci. Lett.*, *278*, 55–66.
- Ryan, W. B. F., et al. (2009), Global multi-resolution topography synthesis, *Geochem. Geophys. Geosyst.*, *10*, Q03014, doi:10.1029/2008GC002332.
- Sandwell, D. T., and W. H. Smith (2009), Global marine gravity from retracked Geosat and ERS-1 altimetry: Ridge segmentation versus spreading rate, *J. Geophys. Res.*, *114*, 1978–2012.
- Scheirer, D. S., and K. C. Macdonald (1993), The variation in cross-sectional area of the axial ridge along the East Pacific Rise: Evidence for the magmatic budget of a fast-spreading center, *J. Geophys. Res.*, *98*, 7871–7885.
- Scheirer, D. S., E. T. Baker, and K. T. M. Johnson (1998), Detection of hydrothermal plumes along the Southeast Indian Ridge near the Amsterdam-St. Paul hotspot, *Geophys. Res. Lett.*, *25*, 97–100.
- Scheirer, D. S., D. W. Forsyth, J. A. Conder, M. A. Eberle, S.-H. Hung, K. T. M. Johnson, and D. W. Graham (2000), Anomalous seafloor spreading of the Southeast Indian Ridge near the Amsterdam-St. Paul Plateau, *J. Geophys. Res.*, *105*, 8243–8262.
- Schilling, J.-G. (1973), Iceland mantle plume: Geochemical evidence along Reykjanes Ridge, *Nature*, *242*, 565–571.
- Sempéré, J.-C., J. R. Cochran, and SEIR Scientific Team (1997), The Southeast Indian Ridge between 88°E and 118°E: Variations in crustal accretion at constant spreading rate, *J. Geophys. Res.*, *102*, 15,489–15,505.
- Small, C. (1995), Observations of ridge-hotspot interactions in the Southern Ocean, *J. Geophys. Res.*, *100*, 17,931–17,946.
- Smith, W. H. F., and D. T. Sandwell (1997), Global sea floor topography from satellite altimetry and ship depth soundings, *Science*, *277*, 1956–1962.
- Stein, C. A., and S. Stein (1994), Constraints on hydrothermal heat flux through the oceanic lithosphere from global heat flow, *J. Geophys. Res.*, *99*, 3081–3095.
- Walker, S. L., E. T. Baker, J. A. Resing, K. Nakamura, and P. D. McLain (2007), A new tool for detecting hydrothermal plumes: An ORP sensor for the PMEL MAPR, *Eos Trans. AGU*, *88*(52), Fall Meet. Suppl., Abstract V21D-0753.
- Wang, T., Y. J. Chen, and C. Tao (2011), Revisit the K-segment of the Southeast Indian Ridge for new evidence of hydrothermal plumes, *Chin. Sci. Bull.*, *56*(1) 1–7, doi:10.1007/s11434-011-4723-5.
- West, M., W. Menke, and M. Tolstoy (2003), Focused magma supply at the intersection of the Cobb hotspot and the Juan de Fuca ridge, *Geophys. Res. Lett.*, *30*(14), 1724, doi:10.1029/2003GL017104.